

## Overview of EAST Experiments on the Development of High-Performance Steady-State Scenario

B.N. Wan<sup>1</sup>, Y.F. Liang<sup>1,2,\*</sup>, X.Z. Gong<sup>1</sup>, N. Xiang<sup>1</sup>, G.S. Xu<sup>1</sup>, Y.W. Sun<sup>1</sup>, L. Wang<sup>1</sup>, J.P. Qian<sup>1</sup>, H.Q. Liu<sup>1</sup>, F.K. Liu<sup>1</sup>, C.D. Hu<sup>1</sup>, Y.P. Zhao<sup>1</sup>, L. Zeng<sup>1</sup>, M. Wang<sup>1</sup>, H.D. Xu<sup>1</sup>, X.J. Wang<sup>1</sup>, L. Zhang<sup>1</sup>, X.J. Zhang<sup>1</sup>, J. Huang<sup>1</sup>, B.J. Ding<sup>1</sup>, Q. Zang<sup>1</sup>, M.H. Li<sup>1</sup>, F. Ding<sup>1</sup>, S.Y. Ding<sup>1</sup>, B. Lyu<sup>1</sup>, Y.W. Yu<sup>1</sup>, T. Zhang<sup>1</sup>, Y. Zhang<sup>1</sup>, G.Q. Li<sup>1</sup> for the EAST team and Collaborators<sup>\*\*</sup>

<sup>1</sup>Institute of Plasma Physics, Chinese Academy of Sciences, Hefei 230031, China

<sup>2</sup>Forschungszentrum Jülich GmbH, Institut für Energie- und Klimaforschung-Plasmaphysik, Partner of the Trilateral Euregio Cluster (TEC), 52425 Jülich, Germany

\*E-mail contact of main author: [y.liang@ipp.ac.cn](mailto:y.liang@ipp.ac.cn)

\*\*See appendix of B.N. Wan et al., *Nucl. Fusion* **55** (2015) 104015

**Abstract.** The EAST research program aims to demonstrate steady-state long-pulse advanced high-performance H-mode operations with ITER-like poloidal configuration and RF-dominated heating schemes. Since last IAEA FEC, EAST has been upgraded with all ITER-relevant auxiliary heating and current drive systems, enabling the investigation of plasma profile control by coupling/integration of various combinations. By means of the 4.6 GHz and 2.45 GHz LHCD systems, H-mode can be obtained and maintained at relatively high density, even up to  $n_e \sim 4.5 \times 10^{19} \text{ m}^{-3}$ , where a current drive effect is still observed. Significant progress has been achieved on EAST, including: *i*). Demonstration of a steady-state scenario (fully non-inductive with  $V_{\text{loop}} \sim 0.0\text{V}$  at high  $\beta_p \sim 1.8$  and high performance ( $H_{98,y2} > 1.0$ ) in upper single-null ( $\epsilon \sim 1.6$ ) configuration with the tungsten divertor; *ii*) Discovery of a stationary ELM-stable H-mode regime with 4.6 GHz LHCD; *iii*) achievement of ELM suppression in slowly-rotating H-mode plasma with the application of  $n = 1$  and 2 RMPs.

### 1. Introduction

Steady-state operation of a future fusion power plant requires the resolution of several issues, in which *i*) a substantial fraction of the plasma current is driven non-inductively by current-drive power and the bootstrap effect; *ii*) robust plasma stability control is required to ensure that the plasma does not exceed operational limits; *iii*) and reliable control of plasma exhaust at high power densities is also required. In addition to those individual issues, the most challenging issue is the coupling or integration of these individual issues into a steady-state scenario with a sufficiently long duration of several particle diffusion times in the PFCs to achieve self-conditioning and particle flux equilibrium operation. However, this has not yet been solved. In order to investigate this issue, EAST has been upgraded with dominant electron heating, low input torque and ITER-like configuration.

Since last IAEA-FEC [1], the exploration of fully non-inductive ( $V_{\text{loop}} \sim 0.0\text{V}$ ), high  $\beta_p \sim 1.8$ , high performance ( $H_{98(y,2)} > 1.0$ ), upper single null ( $\epsilon \sim 1.6$ ) discharges with the tungsten divertor has been successfully demonstrated on EAST. A stationary ELM-stable H-mode regime has been achieved on EAST with 4.6 GHz LHCD. This regime allows nearly fully non-inductive long-pulse ( $> 20\text{s}$ ) operations, exhibiting a relatively high pedestal and good global energy confinement with  $H_{98(y,2)}$  near 1.2, good impurity control, and the capability of operation at relatively high density ( $\bar{n}_e/n_{\text{GW}} \sim 0.5$ ). In the latest experiments, EAST has obtained first long pulse operation on an water-cooled ITER-like tungsten divertor with power handling capability of up to  $10\text{MW/m}^2$  with cassette-type and mono-block technology. A 102 s L-mode discharge and  $\sim 20\text{s}$  H-mode discharges were successfully obtained in USN configuration with RF-dominated heating. This overview will report the main advances in steady-state H mode scenarios since the last IAEA-FEC [1]. The progress on H-modes physics for long pulse operations will also be presented.

## 2. Upgrade and Achievement in support of Long Pulse Advanced Scenarios

Since 2015, EAST has been equipped with all ITER-relevant auxiliary heating and current drive systems, enabling the investigation of plasma profile control by coupling/integration of various sources. In addition, most modern diagnostics have been developed and upgraded to measure the dynamics of plasma profiles, instabilities, and plasma-wall interactions in long-pulse operation. The major upgrades are as follows.

- 1) A 140 GHz long-pulse electron cyclotron resonance heating and current drive (EC RH & CD) system is under development on EAST for the purpose of plasma heating and MHD control [2]. This ECRH system can deliver a total source power of 4 MW into plasma using the second harmonic of the extraordinary mode (X2) for either in stationary operation mode with a pulse length up to 1000 s or a modulation mode with a frequency up to 1 kHz. The actively cooled antenna with front steering mirrors is designed to inject four individually beams over nearly the entire plasma cross section. The launch angle of the beams can be continuously varied over a wide range of over  $30^\circ$  in poloidal direction and  $\pm 25^\circ$  in toroidal direction. To obtain the highest absorption efficiency for different operational scenarios, the beam polarization can also be adjusted during the discharge by turning the orientations of a pair of polarizers in the transmission line. The first EC wave was successfully injected into plasma on EAST in 2015. In addition, H-mode discharges with L-H transition triggered by ECRH injection were obtained and its effects on the electron temperature, particle confinement and the core MHD stabilities, were observed.
- 2) In addition to the previously developed co-current system, the counter-current NBI, which has same designed parameters (80keV, 4MW) with the co-NBI, has been newly installed on EAST in 2015. Up to now, counter NBI successfully obtained the 3.75MW deuterium ion beam during pre-injection test and succeeded in injecting 1.85MW neutral beam. The addition of counter NBI provides unique opportunity to explore the plasma characteristics with high heating power and low momentum input through balanced injection. The results showed that it was possible to study the plasma rotation effect flexibly through varied rotation magnitudes.
- 3) A flexible in-vessel resonant magnetic perturbation (RMP) coil system was installed in 2014 for active MHD instability control in order to achieve long-pulse steady-state operation in the EAST tokamak. It can render a wide range of spectra covering most important configurations of the operating coil systems in present tokamaks and the designed configuration in the future ITER. Consequently, EAST has been capable of investigating ELM control with most existing methods, including RMP, pellet-pacing, SMBI, lower hybrid wave (LHW) and lithium aerosol injection.
- 4) Since last IAEA FEC, EAST diagnostics has progressed significantly to provide high quality experimental data for plasma control, operation, and physics research for the

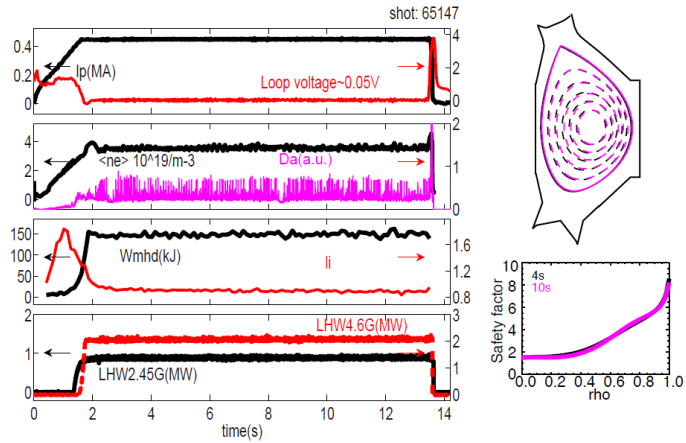


Fig. 1 Time history of several parameters for discharge 65147. a) plasma current & loop voltage; b)  $D_a$  and line averaged density; c) stored energy and internal inductance; d) LHW power; e)-f) overlay of reconstructed shape and  $q$  profile at 4s and 10s.

study on steady-state advanced scenarios [4]. Key profiles like  $T_e$ ,  $n_e$ ,  $T_i$  and rotation are readily available. Especially, an eleven-chord, double-pass, radially-viewing and far-infrared laser-based POLarimeter-INTerferometer (POINT) system has been routinely operated for diagnosing the plasma current and electron density profiles throughout the entire plasma discharge even over 100 seconds, with  $\mu s$  time response able to detect MHD events since 2015 [5]. Fig. 1 shows an example of nearly fully non-inductive H-mode discharge on tungsten divertor. The overlay of  $q$  profiles inferred from EFIT constrained by POINT suggests that a stationary and broad current profile was obtained, which was consistent with  $li$  change in the H-mode phase. For EP and edge physics, fast-Ion D-Alpha spectrum (FIDA) is developed for fast ion behavior and energetic particle related physics [6]. Particular attention has also been devoted to the edge plasmas diagnostics (e.g. Li-BES) [7].

### 3. Exploration of Steady-State Plasma Operation with ITER-like Tungsten Divertor

To develop the fully non-inductive high  $\beta_P$  scenario on EAST with an ITER-like tungsten divertor, NBI and RF power including LHW, ICRF and ECRH were used for heating and current drive. To minimize the flux consumption rate and heat the plasma just after divertor configuration was formed, early LHW injection was utilized during the  $I_p$  ramp-up phase. The outer gap and local gas puffing were gradually optimized for better coupling of RF power into the plasma. In addition, the electron density was increased step by step to avoid the shining-through and fast ion loss when with NBI injection. Using LHW and ECRW, non-inductive long pulse operations up to 102s have been obtained [3]. Both RF waves interact mainly with electrons, resulting in a high central electron temperature of  $\sim 6.0$ keV. The transport barriers formation has been firstly observed in LHCD target plasmas with exclusive electron heating by ECRH. The location of a barrier in  $T_e$  profile responds to the deposition zoned of the ECRH, where ECRH led to the formation of a hot core. Additionally, ICRF was commonly used through fundamental heating of a hydrogen minority in a D majority plasma. For this heating regime, ICRF can create high energy H ions, which Coulomb collisionally slow down on electrons, giving rise to strong electron heating.

Recent experimental explorations of low loop voltage, high  $\beta_P$  scenario for the demonstration of long pulse H-mode operation capability on EAST are performed summarized in Fig. 2. It could be seen that the regime of nearly zero loop voltage is typically obtained at the moderate density, ( $\bar{n}_e \sim 2.5 \sim 3.5 \times 10^{19} m^{-3}$ ). High  $\beta_P$  are accessed with the combined heating of NBI and RF. On EAST, increasing the  $\bar{n}_e$  results in the requirement of more external CD to compensate the reduced LHCD efficiency.

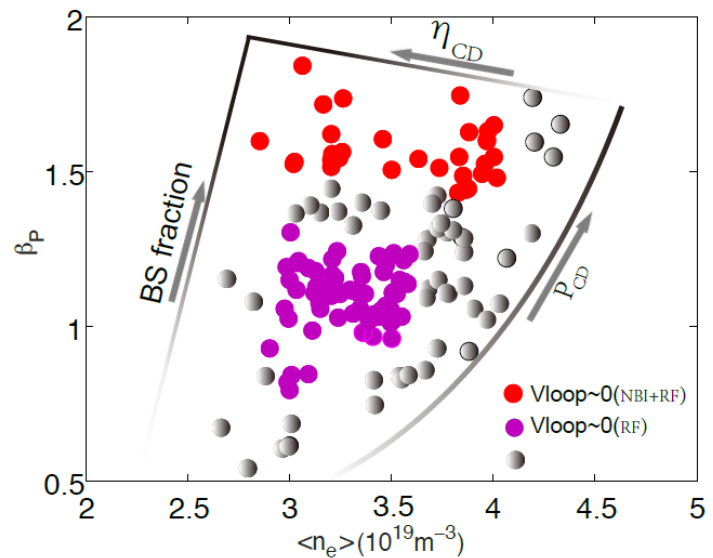


Fig. 2 Scatter plot of EAST  $\beta_P$  versus line-averaged density of low loop voltage plasmas

### Scenario development with NBI and RF heating:

Typical waveforms of a high  $\beta_P$  USN discharge (#62295) are shown in Fig. 3 ( $I_p=0.4\text{MA}$ ,  $B_T=2.2\text{T}$ ,  $R=1.8\text{m}$ ,  $a=0.42\text{m}$ ,  $k=1.7$ ,  $q_{95}\sim 6.6$ ). The injected heating power were  $\sim 2\text{MW}$  NBI,  $\sim 3\text{MW}$  LHW and  $0.5\text{MW}$  ECRH, concurrently. The normalized  $\beta_N\sim 1.3$  and  $\beta_P\sim 1.5$  were reached. Fully non-inductive CD condition was kept constant during the NBI Phase.  $H_{98(y,2)}$  of 1.1-1.2 was achieved with the electron density near 45% of Greenwald density limit. Small grassy ELMs were observed during H-mode phase.

The  $q$  profile was found to be weak sheared with the  $q_{min}>1.5$  inferred from the EFIT code constrained by POINT data [8]. The internal inductance,  $li$  slightly decreased from 0.95 to 0.8 during NBI H-mode phase. The current fractions for the discharge are calculated by TRANSP using experimental profiles. It was found that LHCD fraction reaches up to  $\sim 60\%$ , the bootstrap current fraction is 15%– 25%, the NBI current fraction is  $\sim 15\%$  and only a few percent of the total current is driven by ECRH.

**Scenario development with sole RF heating:** To further explore the RF-dominated heating regime, fully non-inductive discharges were studied with only RF power to possibly extend to long pulse. Fig. 4 showed an H-mode discharge with the sole RF heating and current drive obtained in the 2016 campaign, where the loop voltage was slightly negative. In this discharge,  $I_p=0.45\text{MA}$ ,  $B_T=2.5\text{T}$ ,  $q_{95}\sim 6.0$  and  $\beta_P\sim 1.1$ . The injected power were  $\sim 2.6\text{MW}$  LHW,  $\sim 1\text{MW}$  ICRF and  $0.5\text{MW}$  ECRH. The H-mode pulse length is longer than 15 times the current relaxation time [8] ( $\tau_R\sim 0.4\text{s}$ ), with loop voltage maintained at  $-10\text{mV}$ . From the Faraday rotation measurement shown in Fig. 5, it was confirmed that a stationary current density profile has been obtained in this scenario fully enabled through effective RF heating and CD.

**Hot Spot Issues.** When injecting high LHW power at  $4.6\text{GHz}$ , strong hot spots were often observed on the guard limiter of LHCD antenna by visible CCD

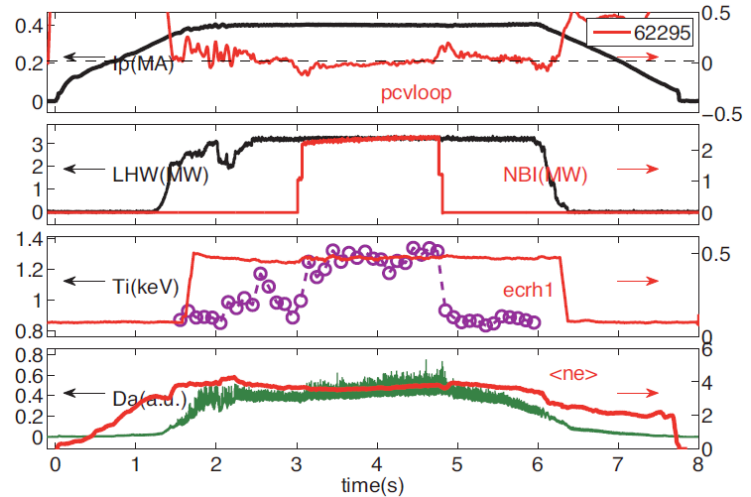


Fig. 3 Time history of several parameters for discharge 62295. a) plasma current & loop voltage; b) LHW& NBI power; c) ECRH power &  $T_i$ ; d)  $Da$  and line averaged density

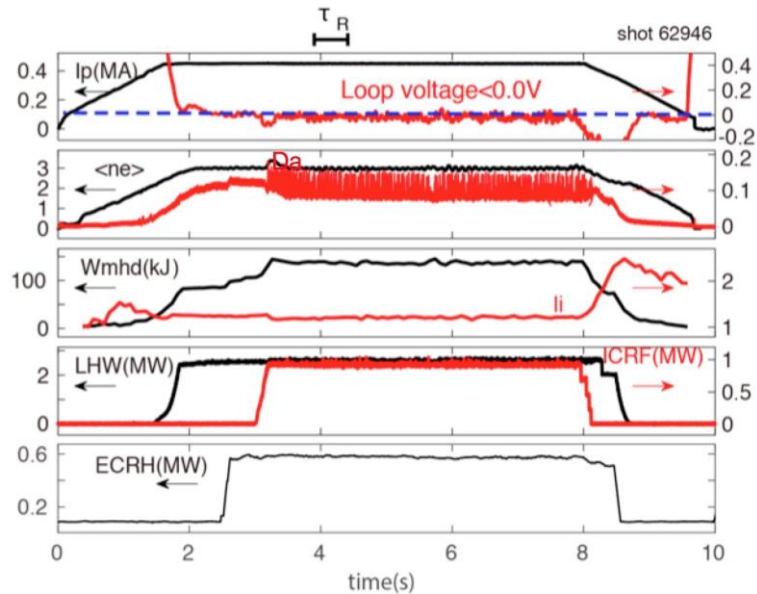


Fig. 4. Time history of several parameters for discharge 62946. a) plasma current & loop voltage; b)  $Da$  and line averaged density; c) stored energy & internal inductance; d) LHW and ICRF power; e) ECRH power

(Fig. 6), leading to a sudden increase of impurity influx such as carbon and copper, and often ending with disruptions. To identify the operation regime with hot spot occurring, a careful scan of global parameters such as plasma density, outer gap and LHW antenna phase difference was performed and the threshold power for the hot spots was around 2.5~3.0MW. The graphite tiles are damaged with the severest region located above the mid-plane. When using the RMP with rotating mode, hot spots could be slightly lightened by tuning the particle flux hitting on the guard limiter. More testing is still ongoing with a new guard limiter design to avoid strong particle flux directly hitting on the limiter.

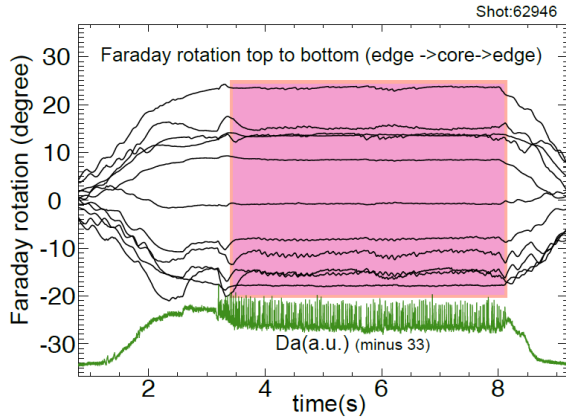


Fig. 5 Time traces of Faraday rotation for discharge 62946.

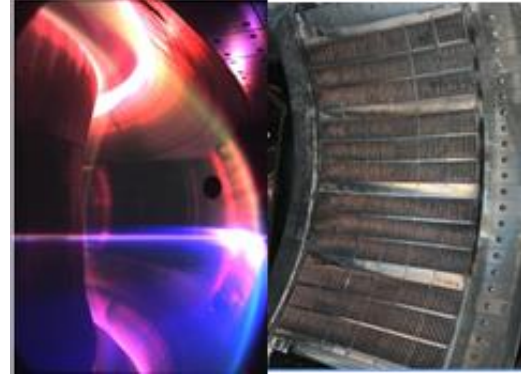


Fig. 6 Hot spot observed by CCD and damage found in the 4.6GHz LHW antenna

## 4. Progress of Key Physics Issues towards Steady-State Operation Regimes

### 4.1. Lower Hybrid Current Drive at High Density

Lower hybrid current drive (LHCD) experiments at high density on EAST aim at fully assessing conditions useful for enabling the LHCD effect into dense plasma core. With the 2.45GHz and 4.6GHz LHCD systems, high density H-mode is obtained and the typical waveforms are shown in Fig. 7, demonstrating the CD capability at high density. The electron cyclotron emission (ECE) signal drops quickly at the L-H transition, implying the decrease of LH driven current, possibly due to the concomitant density increase. Seen from the loop voltage and ECE signal, it is inferred that part of current is driven by LHW even if at the density of  $4.5 \times 10^{19} \text{ m}^{-3}$ . Such density is higher than that of  $1.5\text{-}2.5 \times 10^{19} \text{ m}^{-3}$  obtained by 2.45GHz wave alone [9].

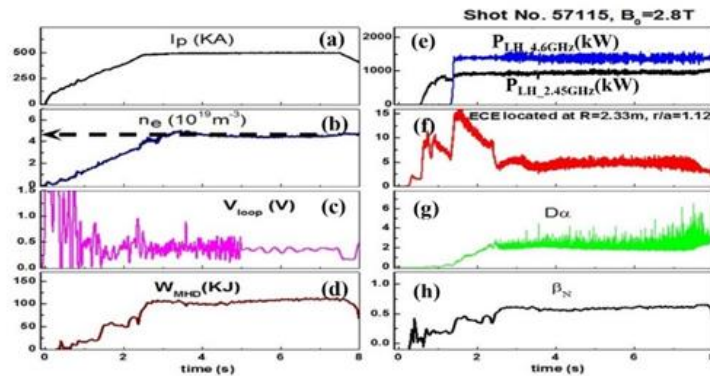


Fig. 7 H-mode with LHCD at high density

To explore long pulse and high performance with LHCD, as shown in Fig. 8, the capability of controlling current profile by optimizing lower hybrid (LH) spectrum with 4.6GHz LHCD system was demonstrated in EAST [10]. Results indicate that the highest current drive (CD) efficiency and the most peaked current density profile occurs with  $N_{//}^{\text{peak}}=2.04$ , suggesting the possibility of profile control by changing the wave spectrum. Previous results [10] showed that LH wave at 4.6 GHz exhibit stronger CD capability than at 2.45 GHz as shown in Fig. 9. As indicated by the parametric instability (PI) measurement by a radio frequency (RF) loop antenna, it is speculated to be mainly ascribed to the less PI behaviour with 4.6GHz LH wave [11]. The effect of LH frequency (2.45 GHz and 4.60 GHz) on PI has been analysed by LHPI

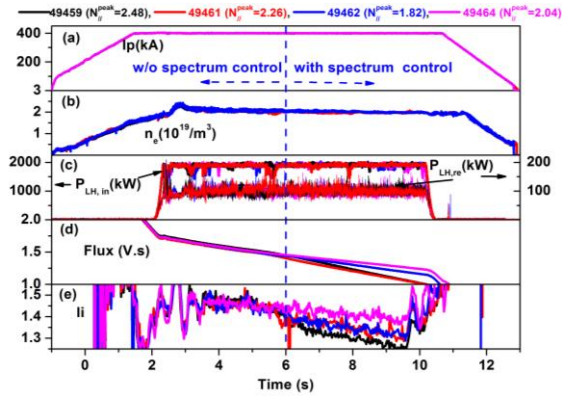


Fig. 8 Effect of LH spectrum on LHCD (4.6GHz)

in comparison with the 4.60 GHz case.

#### 4.2. Pedestal coherent mode and small-ELM H-mode regime at low collisionality

In the recent campaigns, with increased heating power the pedestal collisionality in EAST has been reduced down to  $\nu_e^* < 0.5$ . A new small/no ELM H-mode regime with a low- $n$  (mostly  $n=1$  and sometimes  $n=2$ ) electro-Magnetic Coherent Mode (MCM) at 30-60 kHz as the dominant mode in the pedestal region has been obtained with good confinement,  $H_{98(y,2)} \gtrsim 1.1$  [16]. This regime is different from the Edge Coherent Mode (ECM) characterized small/no ELM H-mode regime observed previously in EAST [17, 18]. ECM is a high- $n$  ( $n \sim 20$ ) electrostatic coherent mode, usually undetectable by fast Mirnov coils mounted on the wall, and has been identified as the Dissipative Trapped Electron Mode (DTEM) [17]. The small/no ELM H-mode regime with MCM appears to be more attractive than that with ECM, since the latter is only obtained at relatively higher pedestal collisionality,  $\nu_e^* \gtrsim 1$ .

[12] and MIT code [13] in Ref. [14], both showing that PI is stronger with 2.45GHz wave. Based on the PI modelling, the LH<sup>star</sup> suite of numerical codes [14, 15] has been further utilised for calculating the driven current profile [14]. Due to the PI effect, the power deposited in the edge region, which cannot contribute to useful LHCD mechanism, is different, leading to a different LH current profile. Such result is qualitatively consistent with the much weaker LHCD effects that are routinely observed on EAST when operating with the 2.45 GHz frequency,

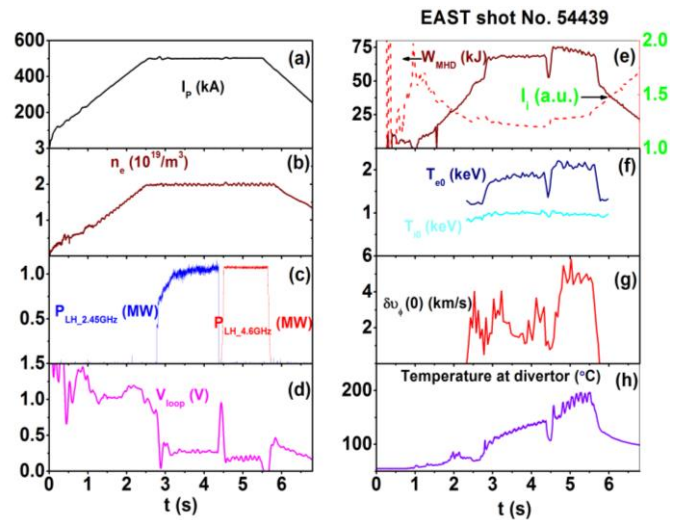


Fig. 9 Typical waveform of LH frequency effect on plasma characteristics

Fig. 10 shows a typical discharge with  $\sim 400$  ms MCM dominated sporadic-small-ELM H-mode phase. In this discharge, the MCM phase is terminated at  $\sim 4$  s by  $n=1$  RMP which leads to a reduction in the pedestal height and stored energy. Then, MCM reappears near 4.25 s as the pedestal height and stored energy recovers. MCM usually appears accompanied by an increase in the divertor  $D_{\alpha}$  emission level, as shown in Fig. 10(d) and stationary light-impurity concentration in the main plasma, which may suggest that MCM helps to exhaust particles across pedestal, thus greatly facilitating stationary H-mode sustainment without large ELMs.

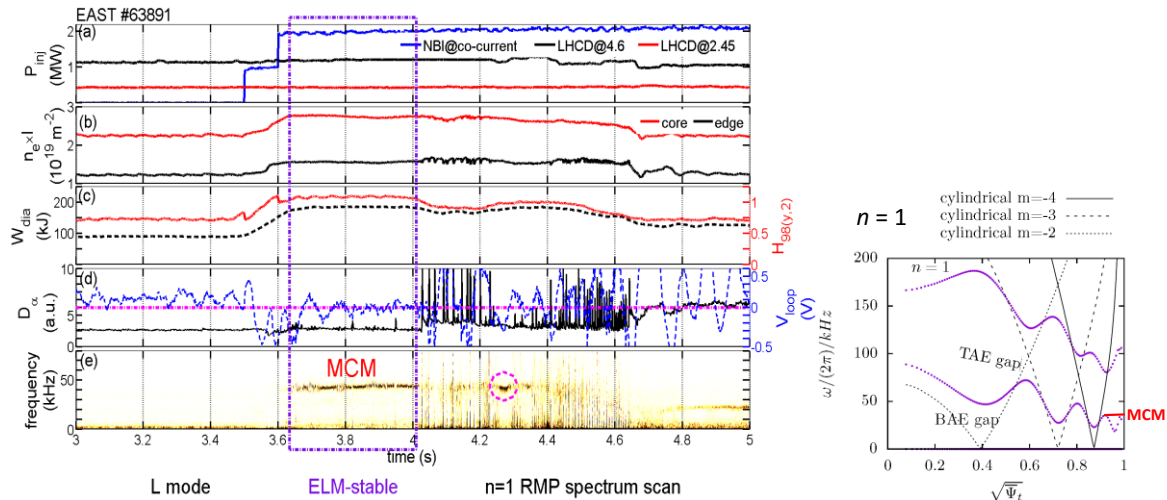


Fig. 10 (Left) A discharge with  $\sim 400$  ms MCM dominated sporadic-small-ELM H-mode phase.  $v_{e,ped}^* < 0.5$ . (Right) an analysis of BAE and TAE gaps using the GTAW code with EAST equilibrium in discharge #62585 at 2.8 s. The QCM frequency is at  $\sim 34$  kHz.

MCM has been measured by several fluctuation diagnostics in the pedestal region, indicating that the MCM is located in the pedestal region, peaks slightly inside the separatrix with a radial correlation length of  $\sim 3$  cm. It propagates in the ELECTRON diamagnetic direction in the lab frame, confirmed by poloidal cross-correlation analysis of Mirnov, lithium BES and mid-plane Langmuir probe signals. MCM appears shortly after the L-H transition when a pedestal forms, as shown in Fig. 10 (left), usually disappears after an ELM crash when the pedestal pressure gradient is reduced, and then reappears as pedestal gradient recovers.

The MCM frequency exhibits a nearly linear dependence with the local Alfvén frequency. An analysis of the Alfvén eigenmode gaps has been conducted using a MHD eigenvalue code GTAW [19]. The MCM frequency appears to be located at the low frequency boundary of Toroidal Alfvén Eigenmode (TAE) gap and near the local trapped-thermal-electron bounce frequency, as shown in Fig. 10 (right), thus pointing to the possibility of trapped-electron-driven TAE mode through bounce resonance with trapped thermal electrons.

### 4.3 ELM control with RMP

To achieve long pulse steady state operation in a tokamak fusion reactor, it is necessary to avoid large transient local heat load on the divertor induced by ELM [20]. Resonant Magnetic Perturbation (RMP) is one the most effective methods for ELM control [21] in present tokamaks and will also be applied on ITER [20]. The physical understanding of ELM suppression and mitigation is limited, and the effect of plasma response to the RMP field on ELM control is under investigation. A flexible RMP system was applied for ELM control after 2014 [22].

Recently, we achieved full ELM control using low  $n$  RMP in low rotating plasma with RF dominant heating on EAST [24]. Fig. 11 shows a discharge for ELM control by using  $n = 1$  RMP in RF heating plasmas. This is a pure RF heating discharge with powers  $P_{\text{LHCD}} = 3$  MW and  $P_{\text{ICRF}} = 1.4$  MW keeping constant. The toroidal rotation near plasma center is very close to 0 ( $< 4$  krad/s), because there is no external momentum input. The toroidal field strength  $B_T = 2.25$  T,  $q_{95} \approx 5.7$ , the plasma current  $I_p = 0.45$  MA and normalized beta,  $\beta_N$  0.8, and the normalized (to bounce or transit frequency of the particle orbit) collisionality near the pedestal top  $v_{e,\text{ped}}^*$  is around 1. ELM frequency increase with RMP coil current. Full ELM suppression has been achieved after the RMP current exceeds a critical value. This is the first demonstration of ELM suppression using low  $n$  RMP in low rotating plasma with RF heating. This might be also benefited from relatively low intrinsic error field [23]. Low  $n$  perturbation may allow a relatively large distance of the RMP coil to plasma, which might be an engineering requirement for future fusion device.

Nonlinear transition between ELM mitigation and suppression was observed during the scan the RMP spectrum by rotating one of the two arrays of RMP coils' current [24]. Fig. 12 shows the nonlinear transition of the plasma response in magnetic field perturbation during the scan of phase difference between upper and lower coils,  $\delta\phi_{\text{UL}}$ , for two periods. ELM suppression is accessed during  $\delta\phi_{\text{UL}} = 50$ - $120^\circ$ . Before ELM suppression there is a phase with strong mitigation during  $\delta\phi_{\text{UL}} = 0$ - $50^\circ$ . In the rest phases, there is only weak mitigation. It is shown that the observed phase of the  $n=1$  response field in the two periods (circles and pluses respectively) is very reproducible. There is a clear nonlinear variation of the response field during the

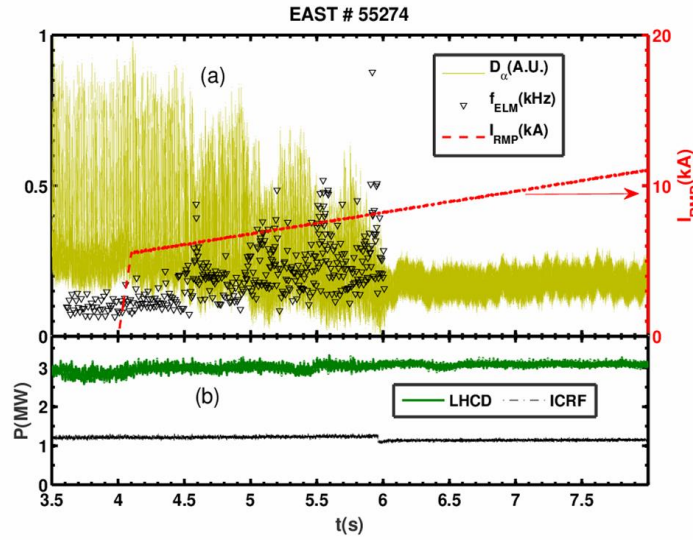


Fig. 11 Full ELM suppression by  $n = 1$  RMP in RF heating plasmas. Temporal evolution of (a) Da emission (solid line), ELM frequency (triangles) and  $n = 1$  RMP coil current (dashed line); (b) heating powers of LHCD (green solid) and ICRF (black dashed).

Nonlinear transition between ELM mitigation and suppression was observed during the scan the RMP spectrum by rotating one of the two arrays of RMP coils' current [24]. Fig. 12 shows the nonlinear transition of the plasma response in magnetic field perturbation during the scan of phase difference between upper and lower coils,  $\delta\phi_{\text{UL}}$ , for two periods. ELM suppression is accessed during  $\delta\phi_{\text{UL}} = 50$ - $120^\circ$ . Before ELM suppression there is a phase with strong mitigation during  $\delta\phi_{\text{UL}} = 0$ - $50^\circ$ . In the rest phases, there is only weak mitigation. It is shown that the observed phase of the  $n=1$  response field in the two periods (circles and pluses respectively) is very reproducible. There is a clear nonlinear variation of the response field during the

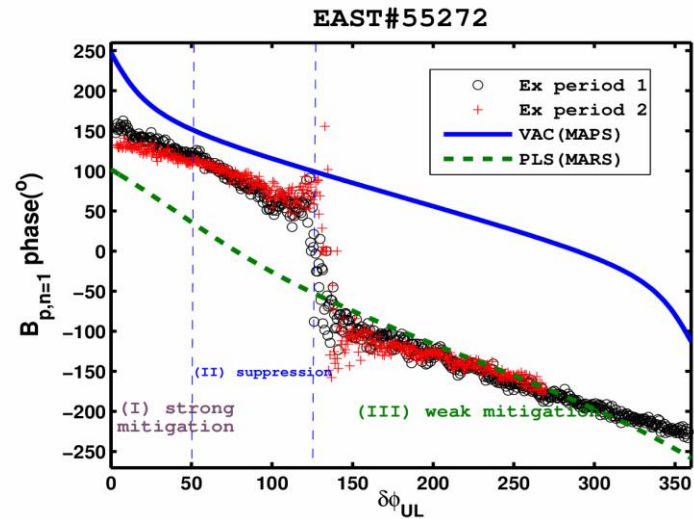


Fig. 12. Nonlinear transition of the plasma response in magnetic field perturbation during the scan of phase difference between upper and lower coils,  $\delta\phi_{\text{UL}}$ , for two periods. Dependence of the phase of the  $n = 1$  response field from observation (circles and plus for the two periods) and the modeling from linear MHD response (dashed line) and vacuum field (solid line)

transition between ELM suppression and mitigation. The observation agrees well with the linear MHD response modeling by using MARS code [25] during weak mitigation phase, while it gradually shifts away and approaches to the vacuum field one modelled by MAPS code [26]. This nonlinear transition in the phase of the response field is linked to the change of edge topology [27]. Footprint splitting in the particle flux during ELM suppression is also consistent with the vacuum field modeling. This observation of nonlinear transition suggests that a critical level of magnetic topological change taking into account plasma response plays a key role in accessing final ELM suppression.

#### 4.4 Heat and Particle Flux Control

Active control of high heat and particle fluxes deposited on the divertor targets is an essential issue for long pulse operations on EAST and future fusion devices, such as ITER. Detailed assessment of divertor in-out asymmetry of particle flux has been made for H-mode plasmas [28] in LSN configuration. For the normal  $B_t$  direction with  $B \times \nabla B \downarrow$ , the divertor plasma features a strong in-out asymmetry with more particle flux to the inner target for all different H-mode phases. Reversing  $B_t$  exhibits a significant impact on the in-out divertor asymmetry. This provides first evidence for the strong influence of SOL drifts on the divertor in-out asymmetry. It is shown that the ion Pfirsch–Schlüter (PS) flow in the SOL accounts for this in-out asymmetry, which is in good agreement with the ion flow measured by reciprocating Mach probes at the outer mid-plane. This in-out particle flux asymmetry results will facilitate the long pulse particle exhaust and density control with cryo-pumps on EAST.

The change of edge magnetic 3D topology, which has been achieved by either LHW heating or RMP coils, is an effective method to handle divertor heat and particle flux deposition. The 3D divertor footprint patterns induced by lower hybrid wave (LHW) [29] and RMP coils [30] have been systematically studied on EAST since the last IAEA FEC through experiments and simulations. Fig. 13 shows the upper outer (UO) divertor particle flux footprints

experimentally measured by divertor Langmuir probe arrays at two different toroidal locations with 4.6GHz LHW of  $\sim 1.6$  MW. By comparing the particle fluxes deposited on divertor targets in the same poloidal location while different toroidal locations, it is clear that the strike point splitting induced by LHW was toroidally asymmetric, exhibiting the 3D divertor footprint pattern. The LHW-induced 3D footprint closely agrees with the modeling using a field line tracing code by taking the helical current filaments in the SOL into account [31]. Fig. 14 shows the experimental and simulated 3D footprints induced by  $n=1$  RMP perturbation during a NBI-heated discharge. The simulations of RMP-induced 3D heat flux footprints on EAST were carried out with EMC3-EIRENE code [30]. Both EMC3-EIRENE simulation (heat flux) and experiment (particle flux) clearly demonstrate the 3D divertor footprint feature with the application of RMP coils. The splitting of strike point changes toroidally. What is truly remarkable is that the simulation shows excellent agreement with the divertor Langmuir probe measurement on the lower outer target in this LSN configuration. In addition, the contours of RMP-induced 3D footprint patterns agree well with

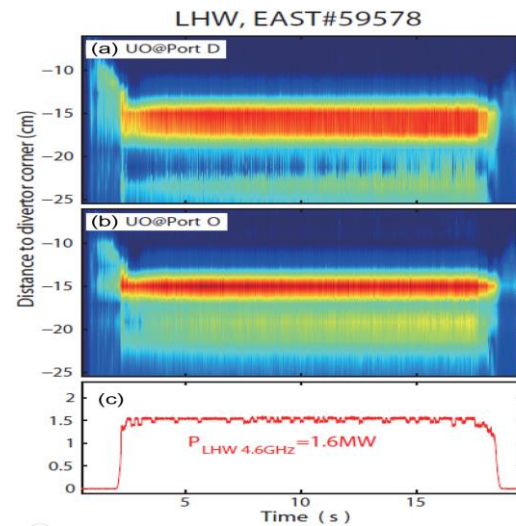


Fig. 13. Contour plots of strike point splitting at two toroidal locations during edge topology induced by 4.6 GHz LHW.

the magnetic footprint results modeled by the TOP2D code basically [32]. For detailed LHW/RMP induced 3D footprint experimental results and experiment-modeling comparison investigation, please refer Ref. [29, 30], respectively. The experimental and modeling results here shall facilitate the particle and heat flux control with tungsten divertor. The integration of 3D power deposition with divertor impurity seeding and/or SMBI are scheduled to simultaneously reduce the heat fluxes at strike point and striated heat flux region, especially for long pulse high performance operations with tungsten divertor.

#### 4.5 Tungsten Accumulation Control

The active control and suppression of tungsten accumulation is now a critical issue for EAST to achieve long pulse high performance operation. The tungsten accumulation study has been then carried out with a newly installed fast response EUV spectrometer [33]. Fig. 15 illustrates two comparable USN H-mode discharges of different ELM frequencies in USN configuration with dominant top tungsten divertor operations. The tungsten impurity signals shown in the bottom panels are normalized to the line-averaged density. It clearly demonstrates that the ELMs can expel the core tungsten impurities effectively at a higher  $f_{\text{ELM}}$ . In shot#63730 of  $f_{\text{ELM}} \sim 90\text{Hz}$ , the tungsten concentration in the plasma core is clearly suppressed during the superimposed phase of  $P_{\text{LHW}@2.45\text{GHz}} = 0.7\text{MW}$  (see  $W^{44+}$  and  $W^{45+}$ ). However, in shot#63722 of a slightly lower  $f_{\text{ELM}} \sim 70\text{Hz}$ , the tungsten accumulation frequently causes periodic H-L back transitions. Note that the H-mode discharge with  $f_{\text{ELM}} \sim 90\text{Hz}$  can be maintained very stably, benefited from the effective relief of core tungsten accumulations. It is also demonstrated in EAST that core tungsten impurity intensity in the H-mode plasmas heated by LHW is much lower than that heated by NBI [34].

#### 5. Summary and Future Plan

To summarize, since the last IAEA-FEC, the research of EAST experiments is mostly focused on the development of high-performance steady-state scenario with RF-dominated heating schemes. The operational window in the steady-state H-mode domain has been extended towards a high  $\beta_{\text{p}}$  regime. Significant progresses in both development of plasma control mechanism and understanding the related physics have been achieved, including:

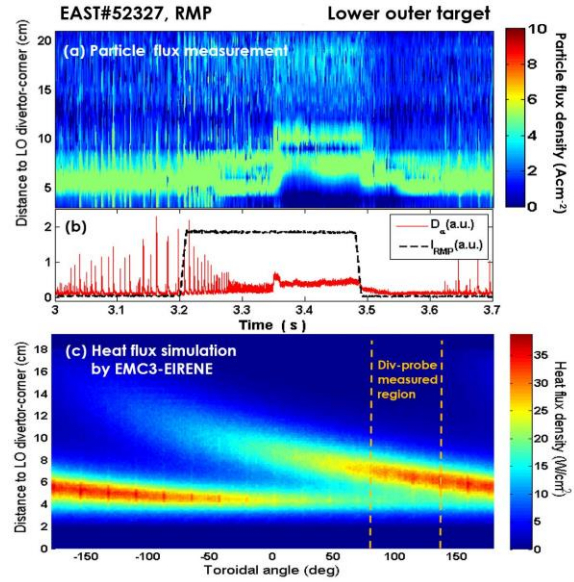


Fig. 14. Contour plots of divertor footprints on lower outer plate for particle flux measurement (a) and heat flux simulation (c) results during RMP (b), with Langmuir probe measured regions shaded.

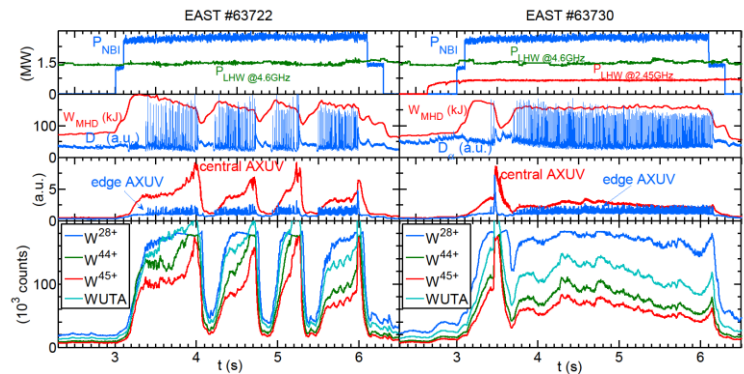


Fig. 15. Comparison of line emission intensities from  $W^{28+}$  ( $48.948\text{\AA}$ ),  $W^{44+}$  ( $60.93\text{\AA}$ ),  $W^{45+}$  ( $62.336\text{\AA}$ ) and  $W\text{-UTA}$  ( $45\text{-}70\text{\AA}$ ,  $W^{27+}\text{-}W^{45+}$ ) in two USN H-mode shots, with  $f_{\text{ELM}, 63722} \sim 70\text{Hz}$  and  $f_{\text{ELM}, 63730} \sim 90\text{Hz}$ .

- Demonstration of a steady-state scenario at high  $\beta_P \sim 1.8$  with the tungsten divertor;
- Discovery of a stationary ELM-stable H-mode regime with 4.6 GHz LHCD;
- Extension of the current drive in high density domain (up to  $4.5 \times 10^{19} \text{ m}^{-3}$ ) with 4.6 GHz LHCD system;
- Achievement of ELM suppression in slowly-rotating H-mode plasma with the application of  $n = 1$  and 2 RMPs;
- Regulating heat deposition distribution and reducing transit peak heat fluxes on the divertor and PFCs by applying 3D magnetic perturbations at the plasma boundary.

In addition to these achievements, the first investigations of both the active control of neoclassical tearing modes (NTMs) and formation of the internal transport barrier (ITB) are performed on EAST for the future development of a steady-state H-mode scenario towards the high  $\beta_N$  regime (see in Fig. 16).

An active NTM control system, which is integrating the real-time mode localization and the feedback control of the steerable ECRH launcher, has been design and developed on EAST. In this system, the island is detected and localized in real time by using Mirnov and ECE signals, and the ECCD deposition position is adjusted through tuning the mirror tilt in the poloidal plane, as well as monitoring the change in the measured magnetic island width, in order to accomplish a good alignment with the magnetic island. Preliminary experimental results showed that the width of the  $m/n=2/1$  islands can be reduced up to 60% of the initial size with application of the ECRH power of 320 kW and deposited near the  $q=2$  surface at  $\rho=0.5$ .

The Internal Transport Barrier (ITB) has been obtained in ELMy H-mode discharges on EAST recently. The ITB discharges are conducted by NBI and LHCD. During the ITB formation, the normalized beta  $\beta_N$  increased from 1.5 to 2, while the  $H_{98(y,2)}$  factor increased from 1 to 1.15. The central ion temperature  $T_i(0)$  increased by 20%, while the central electron temperature  $T_e(0)$  increased by 8% and the line averaged electron density  $\bar{n}_e$  increased by 20%. In addition, a DIII-

D/EAST joint experiment on EAST has successfully demonstrated the broad current profile by varying the deposition profile of the external LHCD, while keeping the plasma in fully-noninductive conditions, which will further strengthen the high beta scenario development for achieving high performance, steady state on EAST in the near future [35].

As of a long term research programme, EAST aims to provide a suitable platform to address physics and technology issues relevant for steady-state advanced high-performance H-mode plasmas with ITER-like configuration, plasma control and heating schemes, i.e., with a flexible selection of double null, lower single null (SN), or upper SN poloidal divertor configurations, ITER-like Tungsten divertor and metal wall, multiple control mechanisms of core and edge MHD behaviours, and divertor power loads control, dominant low momentum input radio frequency heating. Therefore, the experiences and understandings in high-performance long-pulse operation on EAST will be extremely valuable for the next generation machines, i.e. ITER and fusion reactor.

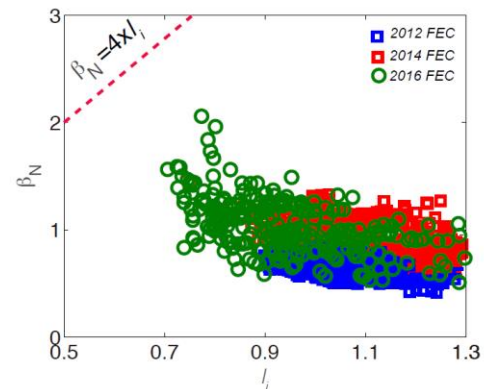


Fig. 16.  $\beta_N$  versus internal inductance (blue/red dashed curves suggests the upper-limit of the operational regime).

### Acknowledgements

This work was supported by National Magnetic Confinement Fusion Science Program of China under Contract Nos. 2013GB106000, 2014GB106000, 2015GB101000, 2015GB102000, 2015GB103000 and National Natural Science Foundation of China under Grant No. 11422546.

### References

- [1] Wan, B.N. et al., Nucl. Fusion **55** (2015) 104015
- [2] Xu, H. et al., Plasma Sci. Technol. **18** (2016) 442
- [3] Qian, J.P. et al., Plasma Sci. Technol. **18** (2016) 457
- [4] Huang, J. et al., "Activities and prospects of US-PRC plasma diagnostic collaboration on EAST" 8th US-PRC Magnetic Fusion Collaboration Workshop, Princeton Plasma Physics Laboratory, June 28-30, 2016.
- [5] Liu, H.Q. et al., J. Instrum. **11** (2016) C01049
- [6] Huang, J. et al., Rev. Sci. Instrum. **87** (2016) 11E542
- [7] Pokol, G.I. et al., "Comparison of HESEL SOL turbulence simulations with BES measurements on EAST", 28th Symposium on Fusion Technology, Prague, Czech Republic, Sep. 5-9, 2016
- [8] Qian, J.P. et al., "EAST equilibrium current profile reconstruction using polarimeter-interferometer internal measurements", submitted to Nucl. Fusion
- [9] Ding B. J. et al., Nucl. Fusion **55** (2013) 113027
- [10] Liu F.K. et al., Nucl. Fusion **55** (2015) 123022.
- [11] Ding B.J., et al, Nucl. Fusion (*accepted*)
- [12] Cesario, R. et al., Nucl. Fusion **54** (2014) 043002
- [13] Baek, S.G. et al., Phys. Plasmas **21** (2014) 061511
- [14] B J Ding et al., Recent experimental and modeling advances in the understanding of lower hybrid current drive in ITER-relevant regimes, EX/P7-5, this conference.
- [15] Cesario R et al., Nat. Commun. **1** (2010) 55
- [16] XU, G.S. et al., "ELM Pace Making and Long-Pulse ELM-Stable H-mode Operation with LHCD in EAST", EX/10-2, this conference
- [17] H.Q. Wang et al Phys. Rev. Lett. **112** (2014) 185004
- [18] H.Q. Wang, G.S. Xu, H.Y. Guo et al Phys. Plasmas **21**, 092511 (2014).
- [19] Y. Hu et al Phys. Plasmas **21**, 052510 (2014).
- [20] R. J. Hawryluk et al., Nucl. Fusion **49**, 065012 (2009).
- [21] T. Evans et al., Phys. Rev. Lett. **92**, 235003 (2004).
- [22] Y. Sun et al., 'Edge localized mode control using  $n = 1$  resonant magnetic perturbation in the EAST tokamak', submitted to Nucl. Fusion (2016)
- [23] Wang, H.H. et al, Nucl. Fusion **56** (2016) 066011
- [24] Sun, Y. et al., Phys. Rev. Lett. **117** (2016) 115001
- [25] Liu, Y. et al, Phys. Plasmas **17** (2010) 122502
- [26] Sun, Y. et al, Plasma Phys. Control. Fusion **57** (2015) 045003
- [27] Reiser, D. and Chandra, D., Phys. Plasmas **16** (2009) 042317
- [28] Liu, J.B. et al, Nucl. Fusion **56** (2016) 066006
- [29] Wang, L. et al., "Evidence and Modeling of 3D Divertor Footprint Induced by Lower Hybrid Waves on EAST with Tungsten Divertor Operations", EX/P7-10, this conference
- [30] Huang, J. et al., "EMC3-EIRENE simulations for the impact of external magnetic perturbations on EAST edge plasma", TH/P6-20, this conference
- [31] Liang, Y. et al., Phys. Rev. Lett. **110** (2013) 235002
- [32] Jia, M.N. et al., Plasma Phys. Control. Fusion **58** (2016) 055010
- [33] Zhang, L. et al., Rev. Sci. Instrum. **86** (2015) 123509
- [34] Zhang, L. et al., "Suppression of tungsten accumulation during ELMy H-mode by lower hybrid wave heating in the EAST tokamak", submitted to Nucl. Mater. Energy
- [35] A. M. Garofalo et al., "Development of high poloidal beta, steady-state scenario with ITER-like W divertor on EAST", EX/4-3, this conference